Deep Crustal Fluid Upwelling through Structural Pathways Observed from Non-active Volcanic Regions, Western Kumamoto, Japan

Takahiro Hosono (hosono@kumamoto-u.ac.jp)
Kumamoto University: Kumamoto Daigaku https://orcid.org/0000-0001-7200-7912
Chikashige Yamanaka
Kumamoto University: Kumamoto Daigaku

Full paper

Keywords: deep fluid, mantle, crust, fault, groundwater, hot spring, carbon isotope

Posted Date: April 1st, 2021

DOI: https://doi.org/10.21203/rs.3.rs-362084/v1

Version of Record: A version of this preprint was published at Earth, Planets and Space on July 29th, 2021. See the published version at https://doi.org/10.1186/s40623-021-01478-1.

Deep crustal fluid upwelling through structural pathways observed from non-active volcanic regions, western Kumamoto, Japan

Takahiro Hosono[a,b]*, Chikashige Yamanaka[c]

[a]Faculty of Advanced Science and Technology, Kumamoto University, 2-39-1 Kurokami, Kumamoto 860-8555, Japan

[b]International Research Organization for Advanced Science and Technology, Kumamoto University, 2-39-1 Kurokami, Kumamoto 860-8555, Japan

[c]Department of Earth and Environmental Science, Faculty of Science, Kumamoto University, 2-39-1 Kurokami, Kumamoto, 860-8555, Japan.

*Corresponding author

E-mail

Takahiro Hosono: hosono@kumamoto-u.ac.jp

Chikashige Yamanaka: yamanaka.c8826@gmail.com

Abstract

Natural springs containing volcanic and magmatic components occur along major volcano-seismotectonic regions over the worlds. However, features of the deep-originated waters were less documented from regions where active volcanic and magmatic activities are not distributed. To characterize the presence of deep fluids of non-volcanic origin 28 groundwater samples (~1,230 m deep) were collected from hot spring sites located at western coast of Kumamoto where the typical subduction related magmatisms are absent. The samples were measured for dissolved ion concentrations and stable isotope ratios (δ^2H_{H2O}, $\delta^{18}O_{H2O}$, $\delta^{13}C_{DIC}$ and $\delta^{34}S_{SO4}$) that were compared with data of 33 water samples from vicinity surface systems. The groundwaters were classified into three types based on major hydrochemistry: high Cl^- fluid, low concentration fluid, and high HCO_3^- fluid. Our dataset suggests that the high Cl^- fluid was formed by saline water mixing with aquifer waters of meteoric origin and subsequently evolved by reverse cation exchange. The low concentration fluid is identical to regional aquifer water of meteoric origin that was subjected to cation exchange. The high HCO_3^- fluid showed the highest HCO_3^-

concentrations (~3,888 mg/l) with the highest $\delta^{13}C_{DIC}$ (-1.9‰). Taking recent geophysical mappings under the study area, we suggest that dissolved carbon was of mantle origin and fluids with high HCO_3^- generated in lower crust were transported towards surface through structural weakness under open tectonic setting. Observed δ^2H_{H2O} and $\delta^{18}O_{H2O}$ shifts support this scenario. The occurrence of deep crustal fluid discharges was sporadic and limited in surface in the study area. Their impacts on surface hydrological systems were minimal except few locations.

Keywords: deep fluid, mantle, crust, fault, groundwater, hot spring, carbon isotope

1. Introduction

Artesian springs with high temperature and/or elevated concentrations occur in major active volcanic and seismotectonic regions globally. These highly concentrated dissolved solutes are facilitated with incorporation of volcanic and magmatic gases and fluids (Aiuppa et al. 2009, 2017), and simultaneous high temperature weathering or alterations that can occur in crust deeper than active hydrological systems in surface (Hedenquist and Lowenstern 1994). Discharge of these fluids is commonly observed in vicinity of active volcano-hydrothermal fields. For example, relevant number of studies tried to depict origins and pathways of deep originated fluids to quantify the impact of volcanic and magmatic activities on lateral material transportations from land to ocean (Chiodini et al. 2000; Dessert et al. 2009; Gaillardet et al. 2011; Rive et al. 2013; Hosono et al. 2018; Perez-Fodich and Derry 2019). Similar high concentration hot spring waters are found in regions where active volcanic and magmatic activities are not existing (Tomaru et al. 2007; Kusuda et al. 2014; Togo et al. 2014; Morikawa et al. 2016; Kusuhara et al. 2020 and references therein), however, origin, distribution, pathway, and thus their impact of hydrochemical features on surface systems are less well known.

The major sources invoked to explain for the origin of deep originated fluids include magmatic fluids, slab fluids and deep crustal fluids (Hedenquist and Lowenstern 1994; Ague 2014; Morikawa et al. 2016). The magmatic fluids present in a crust beneath active volcanoes that are located typically along the volcanic front with some possible exceptions on back arc (Fig. 1a). Dehydration of subducting oceanic plates releases waters and fluids from slab sediments and rocks (here we call slab fluids) into mantle wedges. Some many hot springs in southwest Japan are thought to be originated directly of these fluids on fore

arc system (Tomaru et al. 2007; Kusuda et al. 2014; Togo et al. 2014; Yoshida et al. 2015; Morikawa et al. 2016; Kusuhara et al. 2020). Alternatively, fluids generated in lower crust (here we call deep crustal fluids) can also contribute to surface systems along major pathways especially at regions where substantial heat source exists beneath lower crust such as upwelling asthenospheric mantle (e.g., Zhao et al. 2018), however, this phenomenon has less advocated from nature of lived hot spring discharges due to rare opportunity to test this hypothesis.

Figure 1a shows the depth contours of subducting slabs under Japanese archipelago illustrating that western Kyushu is located on unique setting where possible subduction plate is in mantle deeper than 200 km and typical subduction related magmatisms are absent (Zhao et al. 2021). Some hot springs occur along the coast of western Kumamoto in western Kyushu where none of active volcanic activities distribute (Fig. 1b). Notably, these historically recognized hot springs and other recently developed hot spring facilities are located along and on extension of the major faults (Fig. 1) that possibly allow deep fluids in the crust passing toward surface. There have been no reports comprehensively investigating the origin and formation of these hot springs, however, we thought that precise geochemical characterization on these hot springs may be able to reveal a presence, properties, and discharging processes of the deep crustal fluids.

Stable isotopes are useful for identifying the origin of waters and dissolved ions, and for interpreting the biogeochemical processes in aquifers (Kendall 1998; Cook and Herczeg 2000). Stable isotope ratios of oxygen and hydrogen in the water molecule (δ^2H and $\delta^{18}O$) have been used to examine the contribution of fluids that had experienced high temperature water-rock interaction resulting in $\delta^{18}O$ isotopic shift towards enriched compositions leaving δ^2H unchanged (Giggenbach 1992). Stable carbon isotope ratio of dissolved inorganic carbon ($\delta^{13}C$) is a fundamental tracer for identifying a contribution of magmatic or mantle-derived carbon in fluids (e.g., Chiodini et al. 2000; Yamada et al. 2011; Rive et al. 2013). Sulfur isotope ratio of dissolved sulfate ($\delta^{34}S$) is also applicable for evaluating volcanic influence on spring waters and for interpreting redox processes in aquifer environments (e.g., Kusakabe et al. 2000; Hosono et al. 2014a, 2018). This study integrates the results from these isotopic analyses and characterized geochemical features of hot spring waters with comparison of those from other surface waters for trying to find out the signature of deep crustal fluid upwelling and to assess its impact on surface hydrological systems.

2. Outline of the Study Area

The study area is located on the western coast of the Kumamoto Prefecture in Kyushu Islands and consists of four local domains, Uto, Amakusa, Yatsushiro and Ashikita districts (Fig. 1d). Uto and Amakusa are located on western peninsula and small islands, while Yatsushiro and Ashikita are on western coast of the main island Kyushu, respectively. Coastal flat plain in Yatsushiro is the reclaimed land on tidal flat. The Kyushu has humid subtropical climate and average annual temperature and precipitation of Amakusa and Yatsushiro are 16.4 and 16.8°C and 2,076 and 1,979 mm during 1981-2010, respectively (http://www.jma.go.jp/jma/menu/report.html). Around 40% of total precipitation occurs during summer rainy season in June-July.

In the Kyushu Islands the active volcanoes are generally situated in two major graben structures, Beppu-Shimabara and Kagoshima grabens (Fig. 1b) (Nakada et al. 2016) that are facilitated by unique open tectonic setting partly associated with wet upwelling flow in the mantle wedge (Zhao et al. 2021). The study area is located on just south of the Beppu-Shimabara graben structure, lying between two major active fault systems, Hinagu and Futagawa strike-slip faults (Fig. 1d), for example, which activities generated the 2016 M_w 7.0 Kumamoto destructive earthquakes (e.g., Hosono et al. 2019, 2020). As stated earlier, neither active volcanic activities nor typical subduction related magmatisms are recognized within and beneath the study area. For instance, some recent tomography images (Zhao et al. 2018, 2021) depicted the presence of upwelling asthenospheric mantle in the corner of mantle wedge and there is no major magmas or melts displayed in the crust beneath the study area, which low seismic velocity anomalies are generally observed just beneath active volcanoes like Aso and Kuju (Fig. 1c).

Paleozoic to Mesozoic low-temperature and high-pressure metamorphic rocks and metasedimentary rocks of accretionary prism are widely distributed in the southern part of the Usuki-Yatsushiro Tectonic Line (Fig. 1e). In the northern part of this tectonic line Cretaceous Himenoura Group, alternative sedimentary layers of sandstone, mudstone, shale and conglomerate, comprises of the basement rocks of the study area. Cretaceous metamorphic rocks are also outcropped in Amakusa but their distributions are quite limited. These geological basements are overline by Paleogene sedimentary formations which are further intruded by Miocene dikes and overline by Miocene to Pleistocene volcanic rocks mainly of andesitic to dacitic compositions. Most of these young volcanic rocks are found at Uto peninsula (1.7 to 4.2 Ma; Yokose et al. 2009) and Ashikita district (Fig. 1e). Some limestone formations are interlayered but their distribution is quite limited that are not seen near majority hot spring sites.

3. Samples and Methods

In total 28 groundwater samples were collected from borehole of the hot spring facilities except one sample that was collected from artesian spring during June 2019 and May 2020 (Fig. 1d, Table S1). The depth of borehole is ranging from 70 to 1,230 m and are generally deeper than 800 m and temperature of the waters were ranging from 19.8 to 45.2°C (Table S1). Shallow boreholes (70-100 m) are of Yunoko and Shimoda hot springs, which hot springs with Oyano hot spring were first discovered as artesian flowing from the ground (Fig. 1b) and then later explored subsurface by drilling. Other facilities explored groundwater with elevated temperature though originally there were no hot spring discharge symptoms on a surface land. In addition, 19 stream waters, 10 mountain spring waters, and 4 shallow well (~ 45 m in depth) waters were collected within the same area during July 2019 and April 2020 for isotopic and geochemical comparisons (Fig. 1d), which samples are representative for waters in meteologically-driven surface hydrological systems (we termed 'surface water' for all these waters). No precipitation occurred during 3 days before the sampling.

Groundwaters from hot spring sites were collected directly from the pipes of the pumping or artesian flows. Stream and artesian mountain spring waters were collected on sites, while shallow well waters were obtained using electric pumping or Baylor tube sampler. Field parameters such as temperature, electrical conductivity, pH, oxidation reduction potential, and dissolved oxygen were monitored using field meters (HORIBA D-54) and water samples were collected after these values became constant. The HCO_3^- concentration was determined by *in situ* alkalinity measurement following titrating with sulfuric acid. Water samples were stored in 100, 500 and 2,000 ml polyethylene bottles for major ion concentrations (Na^+, K^+, Ca^{2+}, Mg^{2+}, Cl^-, SO_4^{2-}, and NO_3^-), $\delta^{13}C$ and $\delta^{34}S$ analyses, while 20 ml glass vials were used for collecting water samples for δ^2H and $\delta^{18}O$ analyses, respectively. The samples were filtered through ADVANTEC® 0.2 µm cellulose-acetate filters onsite before storing for 100 ml bottles and immediately after taking back to laboratory for 500 and 2,000 ml bottles, respectively. The filtered water samples in latter two bottles were adjusted to pH 12 to 12.5 with NaOH and to pH 2.5 to 3 with 6 M HCl, respectively, then dissolved inorganic carbon and SO_4^{2-} were collected as $BaCO_3$ and $BaSO_4$ by adding 10% $BaCl_2$ for $\delta^{34}S$ and $\delta^{13}C$ analyses.

Major ion concentrations were measured by ion chromatography (Compact IC 761, Metrohm, Switzerland). Both $\delta^{13}C$ of $BaCO_3$ and $\delta^{34}S$ of $BaSO_4$ were determined using a continuous-flow gas-ratio mass spectrometer (Delta V Advantage, Thermo Fisher Scientific, USA) interfaced with an elemental analyzer (Thermo Fisher Flash 2000, USA)

(Hosono et al. 2014a, 2015). International standards (NBS123 and OGS-1) and several carbonate and sulfate materials were used for quality check of the measurement data. The precision of both $\delta^{13}C$ and $\delta^{34}S$ analyses were generally better than ±0.2‰. The $\delta^{2}H$ and $\delta^{18}O$ of water molecular were determined by a gas-ratio mass spectrometer (Delta V Advantage, Thermo Fisher Scientific, USA) coupled with an automatic water-gas equilibrization devise (Nakano Denshi Co., Ltd., Japan). Based on replicate measurements of standards and samples, the analytical precisions for $\delta^{2}H$ and $\delta^{18}O$ were better than ±0.5‰ and ±0.05‰, respectively.

4. Results and Discussion

4.1. Hydrochemical classification

According to trilinear diagram hydrochemical features of groundwater samples from hot spring sites clearly differ to those for surface waters (Fig. 2a). The surface water samples are broadly plotted on compositional field between Ca-HCO_3^- type with pristine signature and modern sea water, suggesting presence of sea water mixing into fresh surface waters with lower dissolved solutes (electric conductivity of around 50 µS/cm increased near to 1,000 µS/cm, Table S1). On the other hand, the groundwater samples from hot spring sites are exclusively plotted along two different trends with increased concentrations (electric conductivity of ~42,500 µS/cm), high Cl^- with variable Ca^{2+} ratio and high Na^+ with variable HCO_3^- ratio (Fig. 2b). Thus, these groundwaters changed their hydrochemical features owing to several factors including mixing of waters with other origins and geochemical evolutions such as cation exchange and redox processes.

The groundwater samples categorized by the former trend are relatively more enriched in Cl^- and Na^+ and thus we classified this type of waters as High-Cl^- fluid (Fig. 2b and c, Table S1). The groundwater samples categorized by the latter trend are subdivided into two groups, one characterized with greater HCO_3^- concentrations (~3,888 mg/l) and the other with least dissolved concentrations but with relatively higher SO_4^{2-} ratio (Fig. 2d). We classified these two types of groundwaters and named Low-concentration fluid and High-HCO_3^- fluid, respectively (Fig. 2b and d, Table S1). Geographical distribution of three types of fluids, High-Cl^-, Low-concentration and High-HCO_3^- fluids, are shown in Figure 1d. This hydrochemical classification and terminology are used in the following discussion.

4.2. Origin of water

Figure 3 shows δ^2H versus $\delta^{18}O$ diagrams plotting all collected samples and data of some hypothesized source waters for comparison. This comparison allows us to identify the possible origins of water samples of our concern. All surface water samples were closely plotted on local meteoric water line except one stream water sample that is slightly deviated towards composition of modern sea water (Fig. 3a). This suggests that all these waters are mainly of meteoric origin except one sample that was clearly affected by a mixing of sea water. We admit that some of these waters are affected by sea water component in terms of major ion chemistry. However, that effect was small and not obviously reflected on δ^2H and $\delta^{18}O$ shift and thus their compositions were regard as representative feature of waters in surface hydrological systems over the study area.

On Figure 3b, samples of High-Cl^- fluid are broadly plotted along an array between compositional field of surface waters and modern sea water. In combination with Cl^- concentration (Fig. S1), our simple mixing model suggests that this fluid was originated of the surface fresh water admixed with modern sea water with variable mixing proportions ranging from few to nearly 100% due to sea water intrusion and/or contribution of saline pore waters in sediments. This interpretation agrees well with the fact that all High-Cl^- fluids are located just on the coasts or on the reclaimed land in Yatsushiro (Fig. 1d). In turn, for Low-concentration fluid all sample plots were fallen on the compositional field of the surface water (Fig. 3c), indicating their intrinsic meteoric origin analogous to surface circulated waters.

In contrast to High-Cl^- and Low-concentration fluids, some samples of High-HCO_3^- fluid are plotted on right to the local meteoric water line towards hypothesized magmatic water proposed by Giggenbach (1992) (Fig. 3d), although this isotopic shift seems not to be much drastic compared to ones reported from some volcanic fields and other hot spring waters of subduction slab origin (e.g., Kita et al. 2009; Kusuda et al. 2014; Morikawa et al. 2016). Nevertheless, observed isotopic shift possibly indicates incorporation of deep shield fluids that have experienced high temperature water-rock interaction in lower crust particularly in case of our study setting as explained more later.

4.3. Geochemical evolution

4.3.1. Cation exchange

High-Cl^- fluid showing variable Ca^{2+} ratio (Fig. 2b) possibly indicates the occurrence of other processes than source inputs, i.e., geochemical evolution. The chloro-alkaline indices (CAI) (Schoeller 1967) expressed by the flowing equations in milliequivalent concentrations can be used to test the occurrence of cation exchange reactions that control cation concentrations in aquifers.

$$\text{CAI-1} = \frac{Cl^- - (Na^+ + K^+)}{Cl^-} \quad \cdots\cdots\cdots (1)$$

$$\text{CAI-2} = \frac{Cl^- - (Na^+ + K^+)}{Cl^- + SO_4^{2-} + HCO_3^- + NO_3^-} \quad \cdots\cdots\cdots (2)$$

Here, the cation exchange and reverse cation exchange are expected to be occurred when both CAI-1 and CAI-2 show negative and positive values, respectively. These equations are applicable when pH of solutions is lower than 10.3. The pH measured for our samples were all below 10.3 and thus we can test these indices. Figure 4 displayed both CAI-1 and CAI-2 yielded positive values and the values are increased with increase in Ca^{2+} ratio for the High-Cl^- fluid. We can thus conclude that hydrochemical features of High-Cl^- fluid was formed by the sea component mixing and subsequent progressive reverse cation exchange reaction in aquifer. Exchange of calcium ion in exchangeable site in aquifer's solid phase was released by Na^+ in water, assuming to easily be enhanced by additives of saline water with high Na^+ concentration. Moderately, but similar variation in Ca^{2+} ratio was observed for Low-concentration and High-HCO_3^- fluids (Fig. 2). However, both fluids had negative CAI-1 and CAI-2 values which tended to decrease with decrease in Ca^{2+} ratios. Thus, these fluids had evolved along normal cation exchange reaction in contrast to High-Cl^- fluid.

4.3.2. Redox process (sulfur cycle)

The redox process is another important geochemical evolutional process that must be considered. This is true because some groundwaters from hot spring sites showed low dissolved oxygen (< 2 mg/l) and negative oxidation reduction potential (mV) while surface waters generally showed aerobic regime (Table S1). In general, Cl^- concentrations are not affected by redox changes and NO_3^- was not highly concentrated (mostly < 2.0 mg/l except three samples with > 10 mg/l due to local contamination) in the water samples that we investigated (Table S1). Thus additional source characteristics and redox processes will be

discussed hereafter for SO_4^{2-} with conjunction of $\delta^{34}S$ (Fig. 5a). For this, compositional variations for surface waters were considered as juvenile indices that are defined as -7‰ < $\delta^{34}S$ < 15‰ and 2 mg/l < SO_4^{2-} < 30 mg/l, respectively.

On Figure 5b, some High-Cl^- fluids showed elevated SO_4^{2-} (~1,700 mg/l) towards compositions of modern sea water ($\delta^{34}S$: ca. 20.3‰, SO_4^{2-}: ca. 2649 mg/l; Rees et al. 1978), suggesting significant saline water contribution as explained previously. However, other samples showed lower concentrations with elevated $\delta^{34}S$ up to 28‰, indicating an occurrence of microbial reduction of concentrated sulfate of marine origin (Strebel et al. 1990; Tuttle et al. 2009). Some samples were not measured for $\delta^{34}S$ because of their low SO_4^{2-} concentrations probably due to progressive sulfate reduction reaction. Such phenomenon is commonly seen for coastal aquifers either at near to study fields in Kumamoto (Hosono et al. 2014a) or some other countries (Hosono et al. 2010, 2011, 2014b).

The Low-concentration fluid displayed compositions almost identical to those for surface water except two samples with moderately elevated SO_4^{2-} (~280 mg/l) and $\delta^{34}S$ (~17.4‰) and one sample with slightly elevated SO_4^{2-} (~57 mg/l) and depleted $\delta^{34}S$ (~13.7‰) (Fig. 5b). The observed signature for former two samples can be explained by mixing of sulfate of marine origin similar to High-Cl^- fluids but that intensity was too small to clearly be detected on stable isotope ratios of water molecular (Fig. 3c). The signature of later sample can be explained by the oxidation of sulfide with lower $\delta^{34}S$ (Taylor et al. 1984; van Everdingen and Krouse 1985). In summary, overall hydrochemical formation process of Low-concentration fluid resembles to that for surface waters except cation exchange reaction.

The High-HCO_3^- fluid has the least SO_4^{2-} concentrations, which are lower than 16 mg/l, and for majority samples, ranging between detection limit and 5 mg/l (Table S1). Two samples had similar $\delta^{34}S$ compositions to those for surface waters but other four samples showed most enriched $\delta^{34}S$ signature (~45‰) among all samples with depleted SO_4^{2-} concentrations (Fig. 5b). No striking signatures of contribution from marine sulfate are observed, corresponding to results of δ^2H and $\delta^{18}O$ analyses. Overall, hydrochemistry of the High-HCO_3^- fluid was changed their features with similar manner as found for Low-concentration fluid, except less contribution from marine sulfate and tremendous HCO_3^- enrichment (Fig. 2d).

4.4. Deep fluid upwelling

Significant contribution of sulfur from some heat sources was not detected from any water samples collected from our study area (Fig. 5), which $\delta^{34}S$ values resembling to arc volcanic magmas typically in a range between 0 and 10‰ (Ueda and Sakai 1984). On the other hand, elevated HCO_3^- in High-HCO_3^- fluid may be originated of CO_2 gas released from some heat sources that was dissolved in waters and preferentially transported towards surface leaving SO_2 and other gasses (e.g., Ohsawa et al. 2002; Gultekin et al. 2011). The use of $\delta^{13}C$ tracer in dissolved inorganic carbon can provide clue to test this hypothesis (Chiodini et al. 2000; Yamada et al. 2011; Rive et al. 2013).

On the $\delta^{13}C$ versus HCO_3^- concentration diagram (Fig. 6a), all surface water samples fall on $\delta^{13}C$ compositions between -31.3 and -11.8‰ with the lowest HCO_3^- concentrations generally less than ca. 100 mg/l (Table S1), except one sample with relatively elevated $\delta^{13}C$ (-8.9‰) and HCO_3^- concentrations (295 mg/l). These geochemical features are of the typical ecosystem-mediated carbon globally (Clark and Fritz 1997) and aquifer systems near the study areas (Ohsawa et al. 2002; Hosono et al. 2014) and thus are reasonably assigned as a representative composition of surface water systems before alteration by additional source inputs. On the same diagram, almost all groundwater samples from hot spring sites are plotted along the exponential curved trend based on two end-component mixing between hypothesized soil CO_2 and deep originated CO_2, suggesting progressive contribution of CO_2 from deep crust into shallower hydrological systems.

A contribution of deep originated CO_2 dominates in High-HCO_3^- fluid compared to other fluids (High-Cl^- and Low-concentration fluids) which contains only ~5% of carbon from that source (Fig. 6a). Therefore, significant contribution of CO_2 from heat source is responsible for the formation of major hydrochemical features of High-HCO_3^- fluid. Figure 6b displayed geographical distribution of relative contribution of deep originated CO_2. It is notable from this map that groundwaters with the greater contribution are sporadically distributed along the fault systems, and interestingly, these anomalies are characteristically located near the historical hot springs sites, i.e., Yunoko, Shimoda and Oyano, regardless of their host geological formations (Fig. 1). It seems plausible therefore that the presence of relatively young volcanic rocks (Yokose et al. 2009), and presumably still lived magma beneath surface, is not necessarily associated for the occasion of observed deep originated CO_2, instead, another heat source must be more critically important.

Considering geotectonic setting of the study area, upwelling asthenospheric mantle (Zhao et al. 2018, 2021) is the most plausible origin of deep sourced CO_2 that was released into metasomatized lower crust triggered by crustal assimilation with this huge heat source. Similar phenomenon was reported from the Hitoyoshi Basin in non-volcanic regions at western Kumamoto (Fig. 1b) based on the same isotopic systematics (Sakai et al. 2011),

with some additional noble gas isotopes, e.g., $^{3}He/^{4}He$ (Ohsawa et al. 2011). In addition, groundwaters with greater $\delta^{2}H$ and $\delta^{18}O$ compositional shifts tend to be seen on locations where deep originated CO_2 occurs (Fig. 6c and d), supporting above scenario.

Hata et al. (2017, 2020) provided key information for putting more constraint on the realization of the deep crustal fluids. Their recent electrical resistivity image finely identified significant high conductivity blocks exist in western Kyushu under shallow depth (~50 km) in the upper mantle and lower crust, and argued the presence of deep hydrothermal fluids particularly under Hishikari (hydrothermal gold-silver ore deposits) (Fig. 1b), Hitoyoshi, Ashikita and Amakusa, where deep crustal fluid upwelling was anticipated. Thus, we propose fluids generated in a lower crust are the major origin of hypothesized deep fluids, although a possibility of partial involvement of recycled subduction slab fluids can't be neglected as their ultimate origin (Nakamura et al. 2019). However, observed degree of isotopic shift on $\delta^{2}H$ and $\delta^{18}O$ compositions (Fig. 6c) was not much dramatic as seen for deep originated CO_2 contributions (Fig. 6a) probably due to both dispersion of CO_2 gas and mitigation by the mixing with water of meteoric origin while the deep crustal fluids ascent through long distance in the crust.

Discharging slab originated fluids ubiquitous in southwest Japan is thought to be transported through major tectonic structures such as Median Tectonic Line, forearc thrust faults in the accretionary prisms and branching faults, driven by geo- and heat-pressures under compressional tectonic setting (Kusuda et al. 2014; Togo et al. 2014; Yoshida et al. 2015; Morikawa et al. 2016). Deep crustal fluids proposed in this study could ascend also through structural breaks in the Hinagu and Futagawa strike-slip faulting systems (Fig. 1) and possibly in relation to pressure release under open tectonic setting, with a similar law demonstrated from previous works in Kyushu (Hosono et al. 2004, 2018) and from other open tectonic regions (Cerón et al. 1998). It's interesting to note that stronger signature of the deep fluid crustal upwelling (Fig. 6b and d) characteristically occurs near the locations where more than two different faults are crossing (Fig. 1d). This may be due to generation of lower pressure around cross point of the different stresses in the crust where pressurized deep crustal fluids can more easily release towards air pressure near surface (Cappa et al. 2009; Takashima and Kano 2005).

The results of this study showed $\delta^{13}C$ was the most sensible tracers among all measured stable isotope ratios for fingerprinting deep originated components in groundwaters. Giving that the mantle sourced carbon mediated groundwaters (High-HCO_3^- fluid) shared nearly half of total analyzed groundwaters (46%), this type of waters must to be extended wide in space bellow few hundred meters deeper in crust. Despite their prosperity in deep aquifers their discharges to near surface systems look somehow

restrictive only where major fluid pathways exist, and thus, their overall impacts on surface hydrological systems seem to be small on this particular study setting, except only minor contamination with mantle originated carbon, i.e., ca. 5%, observed locally in shallow well water (20 m in depth) near Yunoko hot spring (Fig. 6a). These aspects can be taken when we consider carbon cycle on earth surface systems in other fields.

5. Conclusions

The hydrochemical features of hot spring waters were characterized to understand the origin, distribution and pathway of deep fluids in western Kumamoto using multiple stable isotope ratios ($\delta^{2}H$, $\delta^{18}O$, $\delta^{13}C$ and $\delta^{34}S$) for an area where subduction related active volcanic and magmatic activities are not anticipated. Our results successfully implied the occasion of deep fluid transportation to shallower aquifers along active faults under open tectonic setting, which dissolved carbon and waters are assumed to be originated from upper mantle and lower crust, respectively. This study demonstrates the genesis of some carbon rich hot springs appearing on 'back-arc-side' non-volcanic regions. Additional analysis on noble gas isotopes may provide firmer evidence. The aspects from our results are useful for interpreting data from other fields and for more global generalization, and beneficial to users for hot spring resources.

Abbreviations

MTL: Median Tectonic Line; TL: tectonic line; DIC: dissolved inorganic carbon.

Acknowledgements

We thank the hot spring facilities to kindly let us collect water samples for chemical and isotopic analyses. We are grateful for team members of the Kumamoto University for their cordial help during field survey and laboratory analysis.

Authors' contributions

TH conceived the idea and wrote the manuscript. CY conducted sampling survey and analyzed all dataset. All authors read and approved the final manuscript.

Funding

This study was funded by the JSPS Grant-in-Aid for Scientific Research B (17H01861) and Fostering Joint International Research A (19KK0291).

Availability of data and materials

All data used in this study are listed in figures and Supplementary Information.

Ethics approval and consent to participate

Not applicable.

Consent for publication

Not applicable.

Competing interests

The authors declare no competing interests.

References

Ague JJ (2014) Fluid Flow in the Deep Crust. In: Rudnick RL (ed) The Crust. In: Holland HD, Turekian KK (eds) Treatise on Geochemistry, vol 4. Elsevier Science, Second Edition, pp 203-247

Aiuppa A, Baker D, Webster J (2009) Halogens in volcanic systems. Chem Geol 263:1-18

Aiuppa A, Fischer TP, Plank T, Robidoux P, Di Napoli R (2017) Along-arc, inter-arc and arc-to-arc variations in volcanic gas CO_2/S_T ratios reveal dual source of carbon in arc volcanism. Earth Sci Rev 168:24-47

Cappa F, Rutqvist J, Yamamoto K (2009) Modeling crustal deformation and rupture processes related to upwelling of deep CO_2-rich fluids during the 1965-1967 Matsushiro earthquake swarm in Japan. J Geophys Res 114:B10304. doi:10.1029/2009JB006398

Cerón JC, Pulido-Bosch A, Sanz de Galdeano C (1998) Isotopic identification of CO_2 from a deep origin in thermomineral waters of southeastern Spain. Chem Geol 149:251-258

Chiodini G, Frondini F, Cardellini C, Parello F, Peruzzi L (2000) Rate of diffuse carbon dioxide Earth degassing estimated from carbon balance of regional aquifers: the case of central Apennine, Italy. J Geophys Res Solid Earth 105(B4):8423-8434

Clark ID, Fritz P (1997) Environmental isotopes in hydrogeology. Lewis Publishers, New York

Cook P, Herczeg AL (2000) Environmental Tracers in Subsurface Hydrology. Kluwer Academic Publishers, USA

Dessert C, Gaillardet J, Dupre B, Schott J, Pokrovsky OS (2009) Fluxes of high-versus low-temperature water–rock interactions in aerial volcanic areas: example from the Kamchatka Peninsula, Russia. Geochim Cosmochim Acta 73:148-169

Gaillardet J, Rad S, Rive K, Louvat P, Gorge C, Allègre CJ, Lajeunesse E (2011) Orography-driven chemical denudation in the Lesser Antilles: Evidence for a new feed-back mechanism stabilizing atmospheric CO_2. Am J Sci 311:851-894

Giggenbach WF (1992) Isotopic shifts in waters from geothermal and volcanic systems along convergent plate boundaries and their origin. Earth Planet Sci Lett 113:495-510

Gultekin F, Hatipoglu E, Ersoy AF (2011) Hydrogeochemistry, environmental isotopes and the origin of the Hamamayagi-Ladik thermal spring (Samsun, Turkey). Env Earth Sci 62:1351-1360

Hata M, Munekane H, Utada H, Kagiyama T (2020) Three‐Dimensional Electrical Resistivity Structure Beneath a Volcanically and Seismically Active Island, Kyushu, Southwest Japan Arc. J Geophys Res Solid Earth 125. https://doi.org/10.1029/2019JB017485

Hata M, Uyeshima M, Handa S, Shimoizumi M, Tanaka Y, Hashimoto T, Kagiyama T, Utada H, Munekane H, Ichiki M, Fuji-ta K (2017) 3‐D electrical resistivity structure based on geomagnetic transfer functions exploring the features of arc magmatism beneath Kyushu, Southwest Japan Arc. J Geophys Res Solid Earth 122:172-190. https://doi.org/10.1002/2016JB013179

Hayasaka S (1987) Geologic structure of Kagoshima Bay, South Kyushu, Japan. Assoc Geol Collab Japan 33:225-233 (in Japanese with English abstract)

Hedenquist J, Lowenstern J (1994) The role of magmas in the formation of hydrothermal ore deposits. Nature 370:519-527. https://doi.org/10.1038/370519a0

Hirose F, Nakajima J, Hasegawa A (2008) Three-dimensional seismic velocity structure and configuration of the Philippine Sea slab in southwestern Japan estimated by double-difference tomography. J Geophys Res Solid Earth 113(B9). https://doi.org/10.1029/2007JB005274

Hosono T, Alvarez K, Lin I-T, Shimada J (2015) Nitrogen, carbon, and sulfur isotopic change during heterotrophic (Pseudomonas aerofaciens) and autotrophic (Thiobacillus denitrificans) denitrification reactions. J Contam Hydrol 183:72-81

Hosono T, Delinom R, Nakano T, Kagabu M, Shimada J (2011) Evolution model of $\delta^{34}S$ and $\delta^{18}O$ in dissolved sulfate in volcanic fan aquifers from recharge to coastal zone and through the Jakarta urban area, Indonesia. Sci Total Env 409:2541-2554

Hosono T, Hartmann J, Louvat P, Amann T, Washington KE, West AJ, Okamura K, Böttcher ME, Gaillardet J (2018) Earthquake-induced structural deformations enhance long-term solute fluxes from active volcanic systems. Sci Rep 8:14809. https://doi.org/10.1038/s41598-018-32735-1

Hosono T, Lorphensriand O, Onodera S, Okawa H, Nakano T, Yamanaka T, Tsujimura M, Taniguchi M (2014b) Different isotopic evolutionary trends of $\delta^{34}S$ and $\delta^{18}O$ compositions of dissolved sulfate in an anaerobic deltaic aquifer system. Appl Geochem 46:30-42

Hosono T, Nakano T (2004) Pb-Sr isotopic evidence for contribution of deep crustal fluid of the Hishikari epithermal gold deposit, southwestern Japan. Earth Planet Sci Lett 222:61-69

Hosono T, Siringan F, Yamanaka T, Umezawa Y, Onodera S, Nakano T, Taniguchi M (2010) Application of multi-isotope ratios to study the source and quality of urban groundwater in Metro Manila, Philippines. Appl Geochem 25:900-909

Hosono T, Tokunaga T, Tsushima A, Shimada J (2014a) Combined use of $\delta^{13}C$, $\delta^{15}N$, and $\delta^{34}S$ tracers to study anaerobic bacterial processes in groundwater flow systems. Water Res 54:284-296

Hosono T, Yamada C, Manga M, Wang CY, Tanimizu M (2020) Stable isotopes show that earthquakes enhance permeability and release water from mountains. Nat Commun 11:2776. https://doi.org/10.1038/s41467-020-16604-y

Hosono T, Yamada C, Shibata T, Tawara Y, Wang CY, Manga M, Rahman ATMS, Shimada J (2019) Coseismic groundwater drawdown along crustal ruptures during the 2016 Mw 7.0 Kumamoto earthquake. Water Resour Res 55:5891-5903

Kendall C (1998) Tracing nitrogen source and cycling in catchments. In: Kendall C, McDonnell, JJ (eds) Isotope tracers in catchment hydrology. Elsevier Science B.V., The Netherland, pp 519-576

Kita I, Kai T, Ito R, Ishida M, Ueda A (2009) Magmatic fluid input to the Kuju-Iwoyama hydrothermal system prior to the 1995 eruption of the Kuju volcano (Kyushu, Japan). Geothermics 38:294-302

Kusakabe M, Komoda Y, Takano B, Abiko T (2000) Sulfur isotopic effects in the disproportionation reaction of sulfur dioxide in hydrothermal fluids: implications for the $\delta^{34}S$ variations of dissolved bisulfate and elemental sulfur from active crater lakes. J Volcanol Geotherm Res 97:287-307

Kusuda C, Iwamori H, Nakamura H, Kazahaya K, Morikawa N (2014) Arima hot spring waters as a deep-seated brine from subducting slab. Earth Planets Space 66:119. http://www.earth-planets-space.com/content/66/1/119

Kusuhara F, Kazahaya K, Morikawa N, Yasuhara M, Tanaka H, Takahashi M, Tosaki Y (2020) Original composition and formation process of slab-derived deep brine from Kashio mineral spring in central Japan. Earth Planets Space 72:107. https://doi.org/10.1186/s40623-020-01225-y

Matsumoto Y (1979) Some problems on volcanic activities and depression structures in Kyushu, Japan. Memoir Geol Soc Japan 16:127-139 (in Japanese with English abstract).

Moreno T, Wallis S, Kojima T, Gibbons W (2016) The geology of Japan. Geological Society, London

Morikawa N, Kazahaya K, Takahashi M, Inamura A, Takahashi HA, Yasuhara M, Ohwada M, Sato T, Nakama A, Handa H, Sumino H, Nagao K (2016) Widespread distribution of ascending fluids transporting mantle helium in the fore-arc region and their upwelling processes: Noble gas and major element composition of deep groundwater in the Kii Peninsula, southwest Japan. Geochim Cosmochim Acta 182:173-196

Nakada S, Yakamoto T, Maeno F (2016) Miocene-Holocene volcanism. In: Moreno T, Wallis S, Kojima T, Gibbons W (eds) The geology of Japan. Geological Society, London. pp 237-308

Nakajima J, Hasegawa A (2007) Subduction of the Philippine Sea plate beneath southwestern Japan: slab geometry and its relationship to arc magmatism. J Geophys Res Solid Earth 112(B8). https://doi.org/10.1029/2006JB004770

Nakamura H, Iwamori H, Nakagawa M, Shibata T, Kimura JI, Miyazaki T, Chang Q, Vaglarov BS, Takahashi T, Hirahara Y (2019) Geochemical mapping of slab-derived fluid and source mantle along Japan arcs. Gondwana Res 70:36-49

Ohsawa S, Kazahaya K, Yasuhara M, Kono T, Kitaoka K, Yusa Y, Yamaguchi K (2002) Escape of volcanic gas into shallow groundwater systems at Unzen Volcano (Japan): evidence from chemical and stable carbon isotope compositions of dissolved inorganic carbon. Limnology 3:169-173

Ohsawa S, Sakai T, Yamada M, Mishima T, Yoshikawa S, Kagiyama T (2011) Dissolved inorganic carbon extremely rich in mantle component of hot spring waters from the Hitoyoshi Basin located in a non-volcanic region of central Kyushu, Japan. J Hot Spring Sci 60:410-417

Okumura A, Hosono T, Boateng D, Shimada J (2018) Evaluations of the downward velocity of soil water movement in the unsaturated zone in a groundwater recharge area using δ18O tracer: the Kumamoto region, southern Japan. Geol Croat 71:2. https://doi.org/10.4154/gc.2018.09

Perez-Fodich A, Derry LA (2019) Organic acids and high soil CO_2 drive intense chemical weathering of Hawaiian basalts: Insights from reactive transport models. Geochim Cosmochim Acta 249:173-198

Rees CE, Jenkins WJ, Monster J (1978) The sulfur isotopic composition of ocean water sulphate. Geochim Cosmochim Acta 42:377-381

Rive K, Gaillardet J, Agrinier P, Rad S (2013) Carbon isotopes in the rivers from the Lesser Antilles: origin of the carbonic acid consumed by weathering reactions in the Lesser Antilles. Earth Surf Proc Land 38:1020-1035

Sakai T, Ohsawa S, Yamada M, Mishima T, Yoshikawa S, Kagiyama T, Oue K (2011) Origin of dissolved inorganic carbon of hot spring waters discharged from the non-volcanic region of central Kyusyu, Japan. J Hot Spring Sci 60:418-43

Schoeller H (1977) Geochemistry of groundwater. An international guide for research and practice. UNESCO 15. pp 1-18

Strebel O, Böttcher J, Fritz P (1990) Use of isotope fractionation of sulfate-sulfur and sulfate-oxygen to assess bacterial desulfurication in a sandy aquifer. J Hydrol 121:155-172

Takashima C, Kano A (2005) Depositional processes of travertine developed at Shionoha hot spring, Nara Prefecture, Japan. J Geol Soc Japan 111:751-764

Taylor BE, Wheeler MC, Nordstrom DK (1984) Stable isotope geochemistry of acid mine drainage: experimental oxidation of pyrite. Geochim Cosmochim Acta 48:2669-2678

Togo Y, Kazahaya K, Tosaki Y, Morikawa N, Matsuzaki H, Takahashi M, Sato T (2014) Groundwater, possibly originated from subducted sediments, in Joban and Hamadori areas, southern Tohoku, Japan. Earth Planets Space 66:131. http://www.earth-planets-space.com/content/66/1/131

Tomaru H, Ohsawa S, Amita K, Lu Z, Fehn U (2007) Influence of subduction zone settings on the origin of forearc fluids: Halogen concentrations and $^{129}I/I$ ratios in waters from Kyushu, Japan. Appl Geochem 22:676-691

Tuttle MLW, Breit GN, Cozzarelli IM (2009) Processes affecting $\delta^{34}S$ and $\delta^{18}O$ values of dissolved sulfate in alluvium along the Canadian River, central Oklahoma, USA. Chem Geol 265:455-467

Ueda A, Sakai H (1984) Sulfur isotope study of Quaternary volcanic-rocks from the Japanese Islands Arc. Geochim Cosmochim Acta 48:1837-1848

Yamada M, Ohsawa S, Kazahaya K, Yasuhara M, Takahashi H, Amita K, Mawatari H, Yoshikawa S (2011) Mixing of magmatic CO_2 into volcano groundwater flow at Aso volcano assessed combining carbon and water stable isotopes. J Geochem Explor 108:81-87

Yokose H, Yanashima T, Kikuchi W, Sugiyama N, Shinohara A, Takeuchi T, Nagao K, Kodama K (2009) Episodic magmatism since 5Ma in the western part of Beppu-Shimabara graben, Kyusyu, Japan. J Mineral Petrol Econ Geol 94:338-348 (in Japanese with English abstract)

Yoshida K, Hirajima T, Ohsawa S, Kobayashi T, Mishima T, Sengen Y (2015) Geochemical features and relative B–Li–Cl compositions of deep-origin fluids trapped in high-pressure metamorphic rocks. Lithos 226:50-64

Zhao D, Wang J, Huang Z, Liu X (2021) Seismic structure and subduction dynamics of the western Japan arc. Tectonophysics 802:228743. https://doi.org/10.1016/j.tecto.2021.228743

Zhao D, Yamashita K, Toyokuni G (2018) Tomography of the 2016 Kumamoto earthquake area and the Beppu-Shimabara graben. Sci rep 8:15488. https://doi.org/10.1038/s41598-018-33805-0

van Everdingen RO, Krouse HR (1985) Isotope composition of sulphates generated by bacterial and abiological oxidation. Nature 315:395-396

Figure Captions

Fig. 1 Map showing the study area and its geological background. **a** Tectonic setting of the Japanese archipelago with locations of active volcanoes (triangle). Red and blue lines show the depth contours of Pacific and Philippine Sea subducting plates, respectively (Nakajima and Hasegawa 2007; Hirose et al. 2008). Blue dotted line indicates extension of deep subduction of Philippine Sea slab (Zhao et al. 2021). **b** Tectonic structure of the Kyushu Islands with some important localities explained in the main text. The Beppu-Shimabara and Kagoshima grabens are after Matsumoto (1979) and Hayasaka (1987). Yellow hatch indicates an area where subsurface high conductivity blocks distribute in and beneath lower crust which were depicted from recent electrical resistivity survey (Hata et al. 2017). **c** The A-A' cross section in panel **b** showing low seismic velocity zones in the mantle wedge and crust (Zhao et al. 2018). **d** Sampling locations shown on topographical map with locality name and major fault systems. **e** Simplified geological map modified after Moreno et al. (2016). Geographical distribution of three types of fluids, High-Cl^-, Low-concentration and High-HCO_3^- fluids, are also shown.

Fig. 2 Hydrochemical classification based on trilinear diagram. **a** Comparison between surface waters and groundwaters from hot spring sites. **b** Classification of three different types of groundwaters from hot spring sites. **c** Difference in Cl^- concentrations among three types of fluids. **d** Diversity in HCO_3^- concentrations among three types of fluids.

Fig. 3 δ^2H versus $\delta^{18}O$ diagrams. **a-d** Isotopic signatures for High-Cl^- fluid, Low-concentration, and High-HCO_3^- fluids, respectively, with comparison of those for surface waters. Isotopic compositional field for hypothesized magmatic water is after Giggenbach (1992). Local meteoric water line in Kumamoto (ca. 20 km northeast from Uto district) are after Okumura et al. (2018).

Fig. 4 Biplot diagram between Ca^{2+} ratio and chloro-alkaline indices (CAI-1 and CAI-2) for three types of groundwaters from hot spring sites, High-Cl^- fluid, Low-concentration, and High-HCO_3^- fluids. Ca^{2+} ratio denotes proportion of calcium ion among four major cations (Na^+, K^+, Ca^{2+} and Mg^{2+}) in milliequivalent concentrations.

Fig. 5 SO_4^{2-} concentration versus $\delta^{34}S$ diagrams. Sample plots for three types of groundwaters from hot spring sites (High-Cl^- fluid, Low-concentration, and High-HCO_3^-

fluids), with comparison of those for surface waters. Compositions of modern sea water are after Rees et al. (1978).

Fig. 6 Identification for deep crustal fluids. **a** HCO_3^- concentration versus $\delta^{13}C$ diagram for all collected water samples. Simple two components mixing curved lines with relative contribution rates from mantle sourced carbon in 10% interval are shown in the graph. Mixing of two sets of end-components, soil carbon (HCO_3^- and $\delta^{13}C$: 20 mg/l and -30‰, 160 mg/l and -30‰, respectively) and mantle sourced carbon (HCO_3^- and $\delta^{13}C$: 4,000 mg/l and -4.5‰, 4,000 mg/l and -1.5‰, respectively), were hypothesized taking compositional variations observed from this study, with a same method applied elsewhere (e.g., Chiodini et al. 2000; Yamada et al. 2011; Rive et al. 2013). **b** Geographical distribution of relative contribution from mantle sourced carbon in groundwater samples deduced from mixing model shown in panel **a**. **c** δ^2H versus $\delta^{18}O$ plot diagram for High-HCO_3^- fluids shown in different colors with variable $\delta^{18}O$. **d** Geographical distribution of $\delta^{18}O$ values. The symbol color is same as in panel **c**.

Table S1 Location, property, and measurement and analytical results for all water samples collected in this study from western coast of Kumamoto in western Kyushu, Japan.

Fig. S1 Cl^- concentration versus δ^2H diagram for High-Cl^- fluids. Simple two components (surface water and modern sea water) mixing lines with relative contribution rates from modern sea water in 10% interval are shown. End-component for surface water with variable compositions (Cl^- and δ^2H: 13.8 mg/l and -52.6‰ ~ 17.2 mg/l and -37.3‰) were considered.

Figures

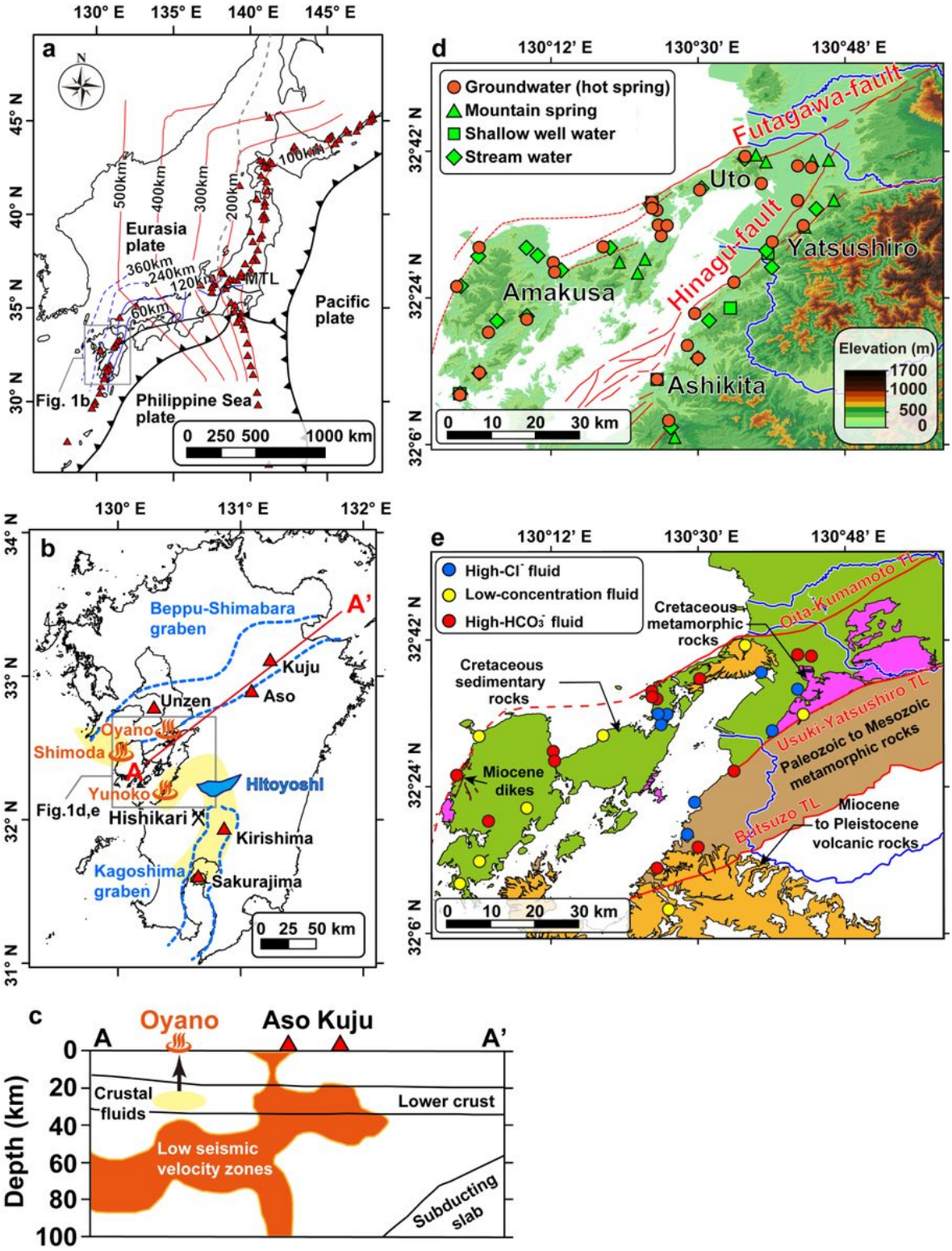

Figure 1

Map showing the study area and its geological background. a Tectonic setting of the Japanese archipelago with locations of active volcanoes (triangle). Red and blue lines show the depth contours of Pacific and Philippine Sea subducting plates, respectively (Nakajima and Hasegawa 2007; Hirose et al.

2008). Blue dotted line indicates extension of deep subduction of Philippine Sea slab (Zhao et al. 2021). b Tectonic structure of the Kyushu Islands with some important localities explained in the main text. The Beppu-Shimabara and Kagoshima grabens are after Matsumoto (1979) and Hayasaka (1987). Yellow hatch indicates an area where subsurface high conductivity blocks distribute in and beneath lower crust which were depicted from recent electrical resistivity survey (Hata et al. 2017). c The A-A' cross section in panel b showing low seismic velocity zones in the mantle wedge and crust (Zhao et al. 2018). d Sampling locations shown on topographical map with locality name and major fault systems. e Simplified geological map modified after Moreno et al. (2016). Geographical distribution of three types of fluids, High-Cl-, Low-concentration and High-HCO3- fluids, are also shown. Note: The designations employed and the presentation of the material on this map do not imply the expression of any opinion whatsoever on the part of Research Square concerning the legal status of any country, territory, city or area or of its authorities, or concerning the delimitation of its frontiers or boundaries. This map has been provided by the authors.

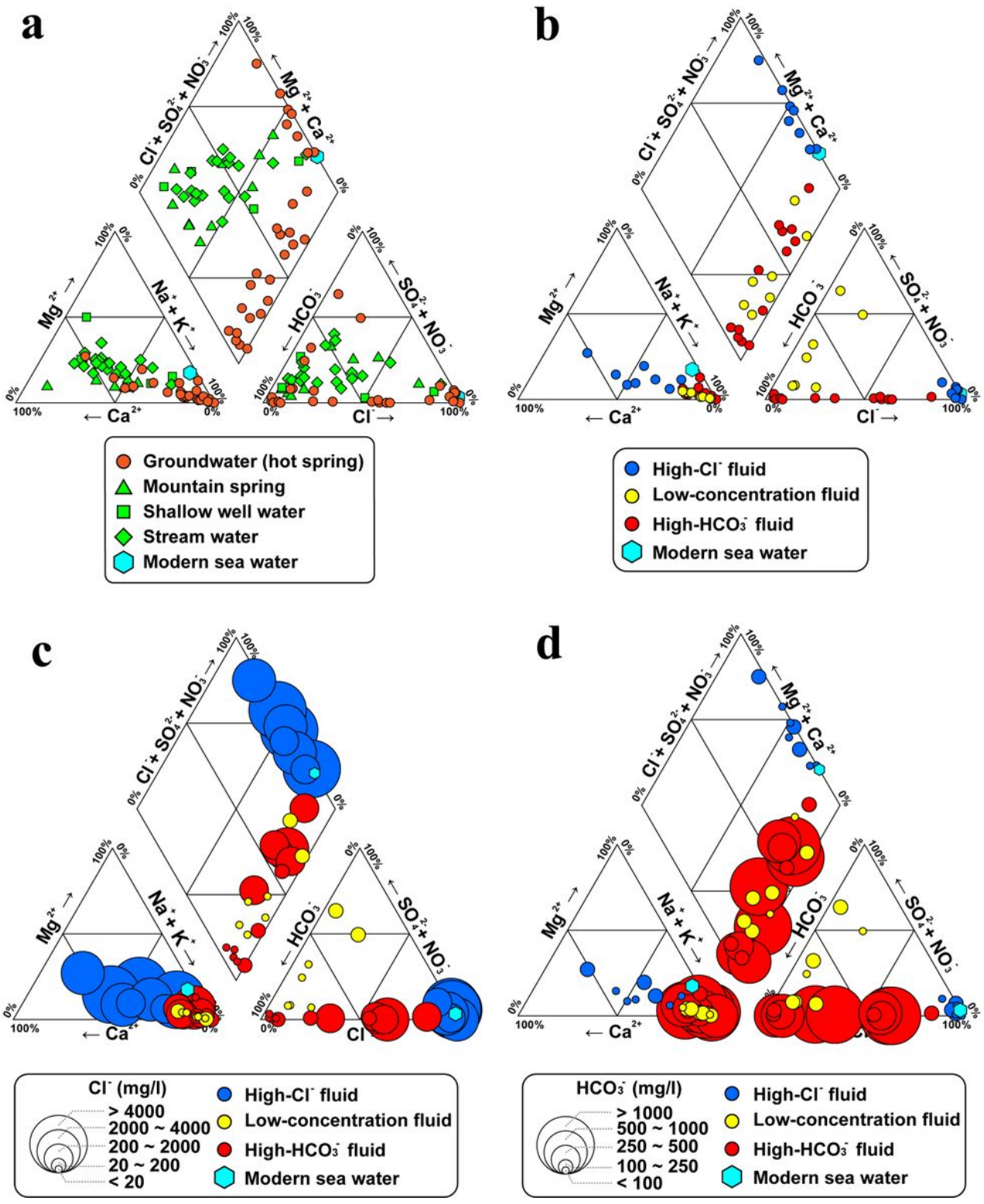

Figure 2

Hydrochemical classification based on trilinear diagram. a Comparison between surface waters and groundwaters from hot spring sites. b Classification of three different types of groundwaters from hot spring sites. c Difference in Cl- concentrations among three types of fluids. d Diversity in HCO3- concentrations among three types of fluids.

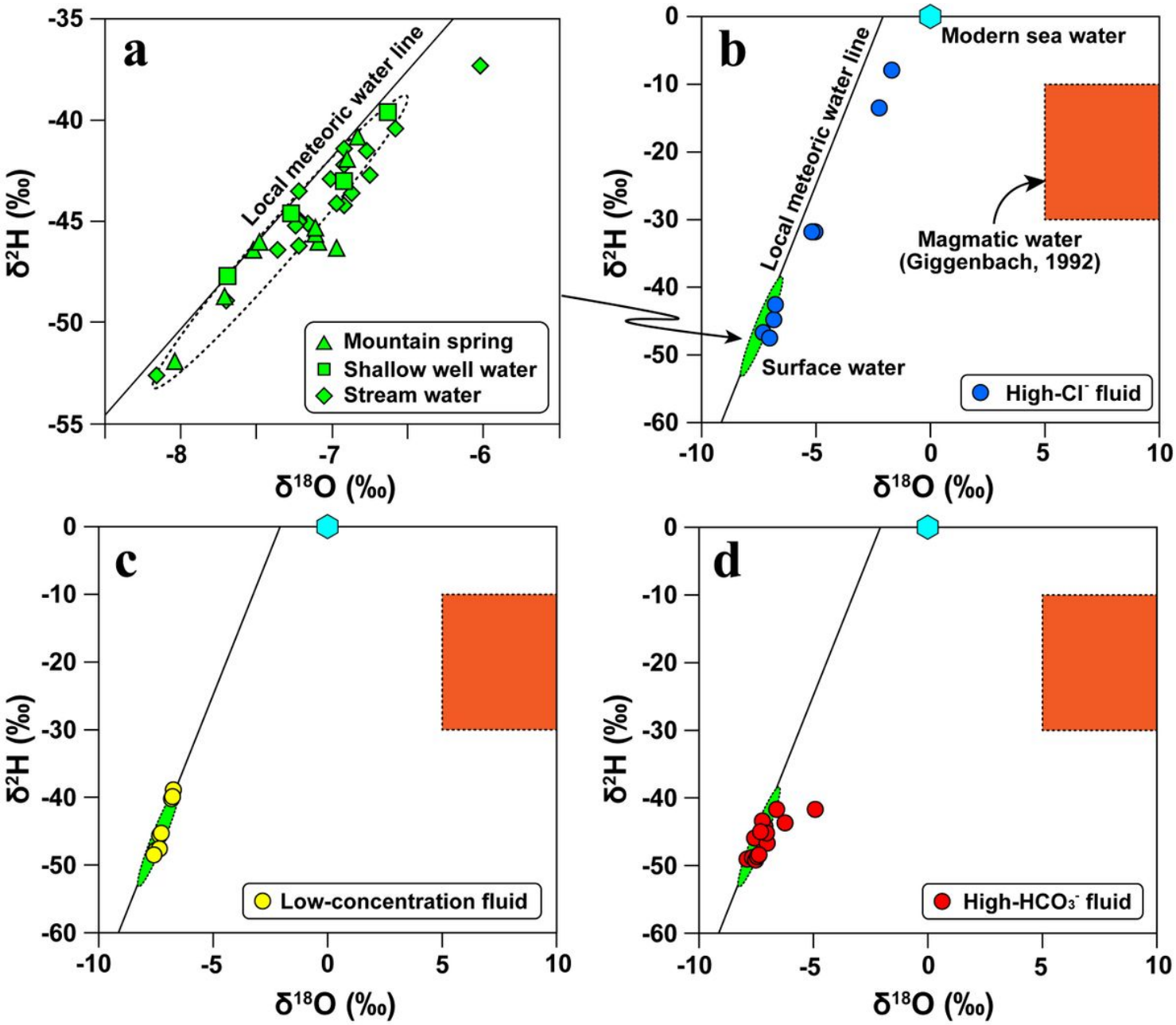

Figure 3

δ2H versus δ18O diagrams. a-d Isotopic signatures for High-Cl- fluid, Low-concentration, and High-HCO3- fluids, respectively, with comparison of those for surface waters. Isotopic compositional field for hypothesized magmatic water is after Giggenbach (1992). Local meteoric water line in Kumamoto (ca. 20 km northeast from Uto district) are after Okumura et al. (2018).

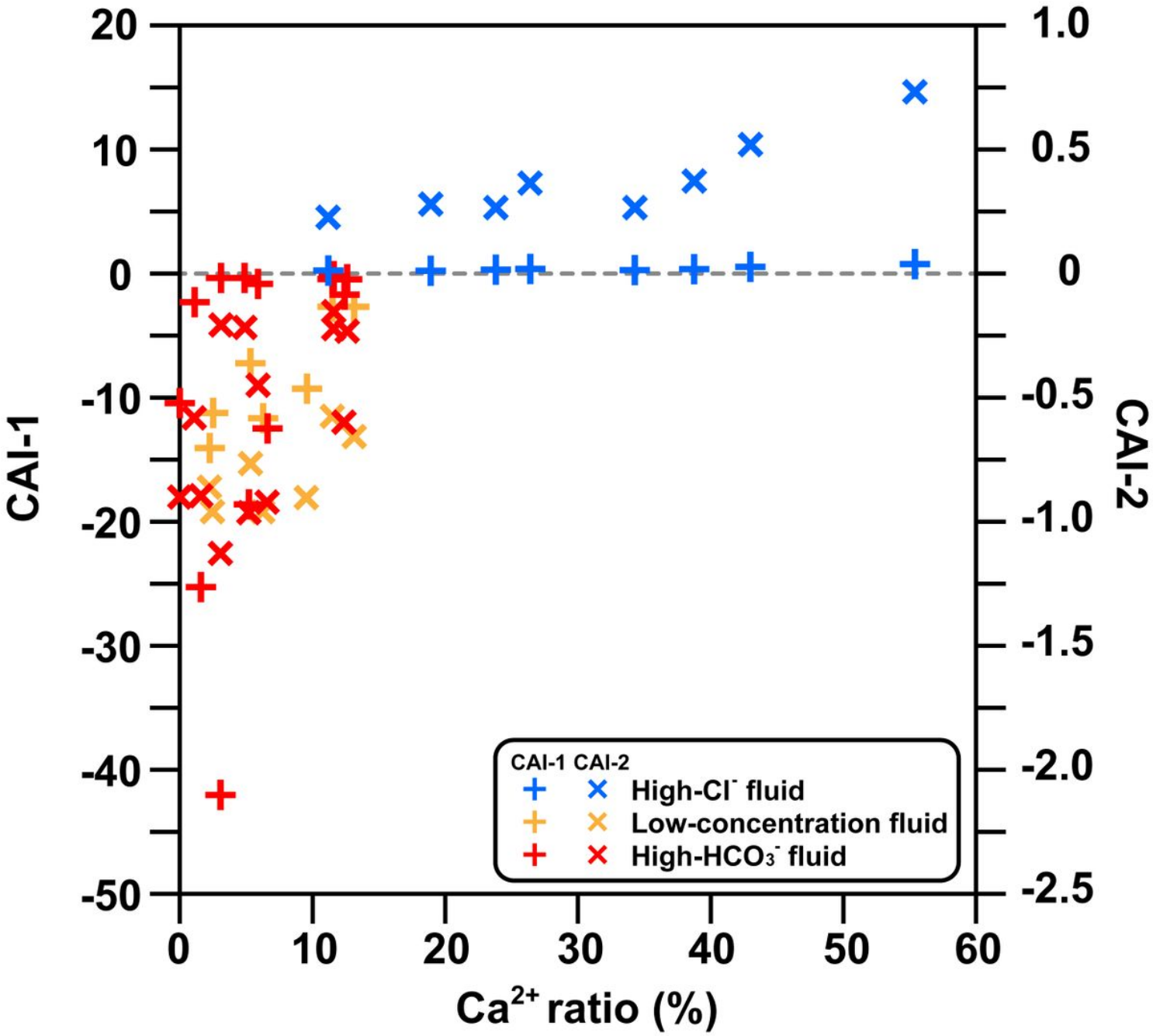

Figure 4

Biplot diagram between Ca2+ ratio and chloro-alkaline indices (CAI-1 and CAI-2) for three types of groundwaters from hot spring sites, High-Cl- fluid, Low-concentration, and High-HCO3- fluids. Ca2+ ratio denotes proportion of calcium ion among four major cations (Na+, K+, Ca2+ and Mg2+) in milliequivalent concentrations.

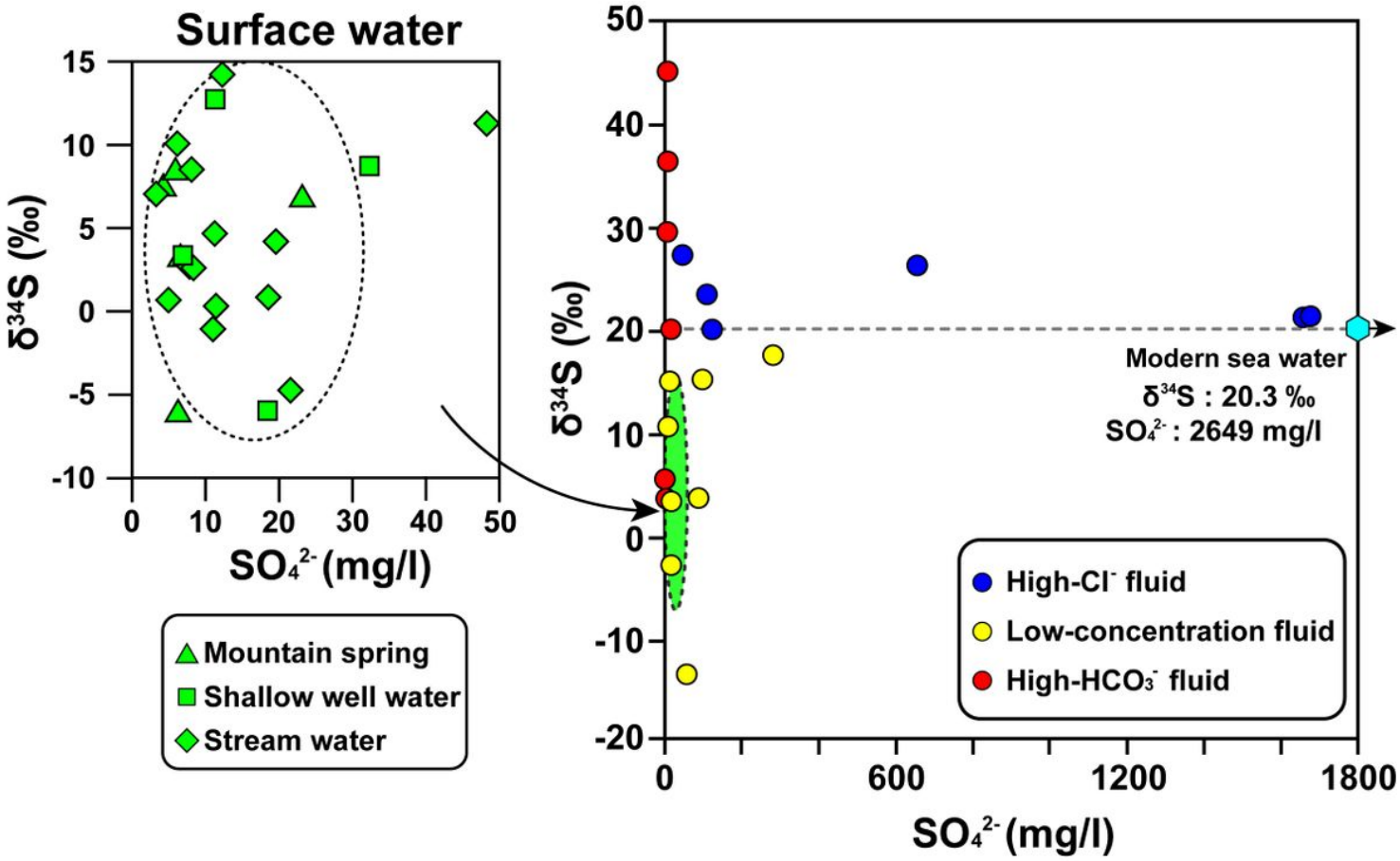

Figure 5

SO42- concentration versus δ34S diagrams. Sample plots for three types of groundwaters from hot spring sites (High-Cl- fluid, Low-concentration, and High-HCO3- fluids), with comparison of those for surface waters. Compositions of modern sea water are after Rees et al. (1978).

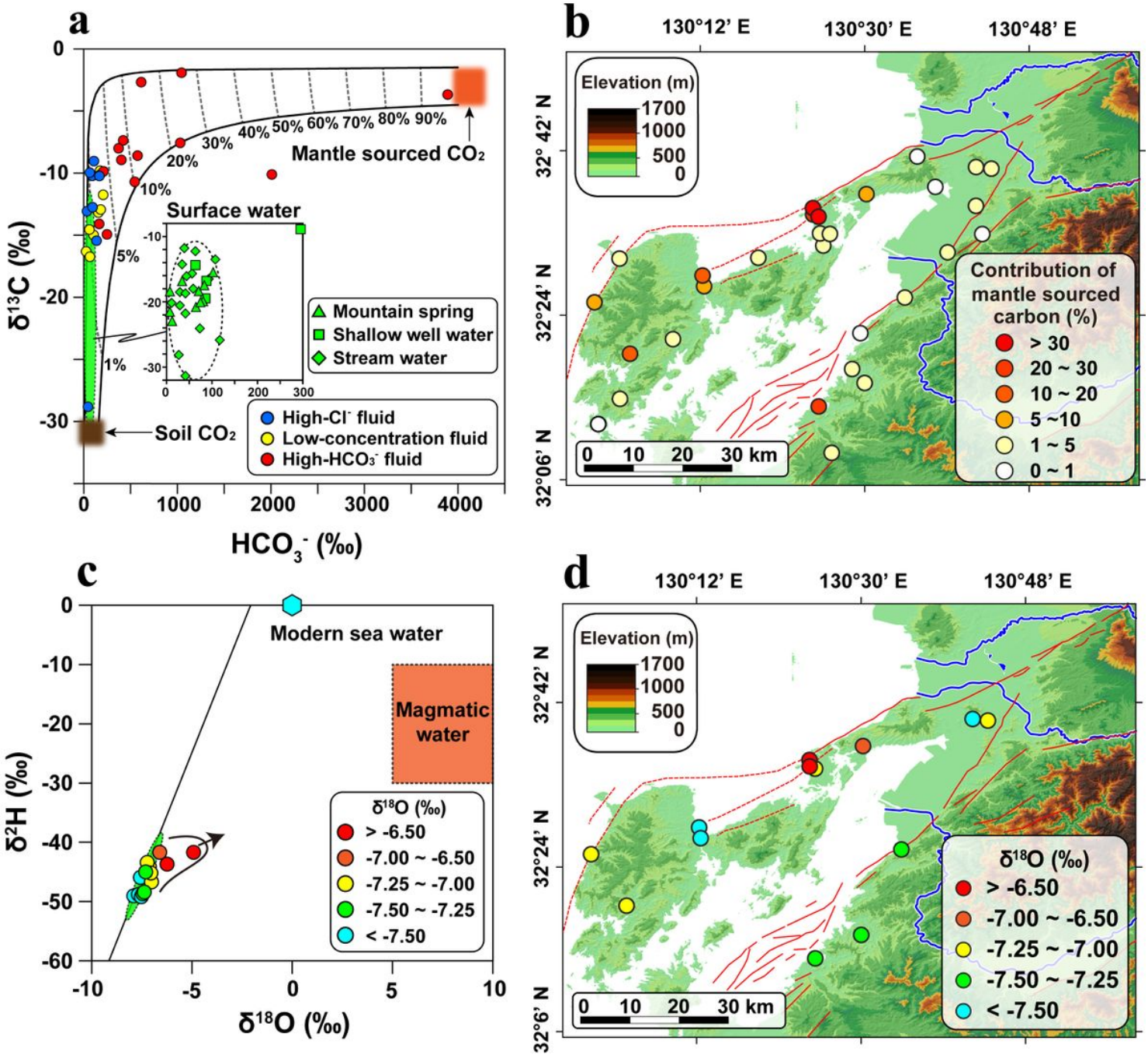

Figure 6

Identification for deep crustal fluids. a HCO3- concentration versus δ13C diagram for all collected water samples. Simple two components mixing curved lines with relative contribution rates from mantle sourced carbon in 10% interval are shown in the graph. Mixing of two sets of end-components, soil carbon (HCO3- and δ13C: 20 mg/l and -30‰, 160 mg/l and -30‰, respectively) and mantle sourced carbon (HCO3- and δ13C: 4,000 mg/l and -4.5‰, 4,000 mg/l and -1.5‰, respectively), were hypothesized taking compositional variations observed from this study, with a same method applied elsewhere (e.g., Chiodini et al. 2000; Yamada et al. 2011; Rive et al. 2013). b Geographical distribution of relative contribution from mantle sourced carbon in groundwater samples deduced from mixing model shown in panel a. c δ2H versus δ18O plot diagram for High-HCO3- fluids shown in different colors with variable

δ18O. d Geographical distribution of δ18O values. The symbol color is same as in panel c. Note: The designations employed and the presentation of the material on this map do not imply the expression of any opinion whatsoever on the part of Research Square concerning the legal status of any country, territory, city or area or of its authorities, or concerning the delimitation of its frontiers or boundaries. This map has been provided by the authors.

Supplementary Files

This is a list of supplementary files associated with this preprint. Click to download.

- Fig.S1.jpg
- Graphicabstract.jpg
- TableS1.xlsx